ACS chemical biology

Articles

pubs.acs.org/acschemicalbiology

Effective GTP-Replacing FtsZ Inhibitors and Antibacterial Mechanism of Action

Marta Artola,[†] Laura B. Ruiz-Avila,[‡] Albert Vergoñós,[‡] Sonia Huecas,[‡] Lidia Araujo-Bazán,[‡] Mar Martín-Fontecha,[†] Henar Vázquez-Villa,[†] Carlos Turrado,[†] Erney Ramírez-Aportela,[‡,§] Annabelle Hoegl,[∥] Matthew Nodwell,[∥] Isabel Barasoain,[‡] Pablo Chacón,[§] Stephan A. Sieber,[∥] Jose M. Andreu,[‡] and María L. López-Rodríguez*[,†]

[†]Departamento de Química Orgánica I, Facultad de Ciencias Químicas, Universidad Complutense de Madrid, E-28040 Madrid, Spain

[‡]Centro de Investigaciones Biológicas, CSIC, E-28040 Madrid, Spain

[§]Instituto de Química-Física Rocasolano, CSIC, E-28006 Madrid, Spain

[∥]Center for Integrated Protein Science Munich, Technische Universität München, Department of Chemistry, D-85747 Garching, Germany

Supporting Information

ABSTRACT: Essential cell division protein FtsZ is considered an attractive target in the search for antibacterials with novel mechanisms of action to overcome the resistance problem. FtsZ undergoes GTP-dependent assembly at midcell to form the Z-ring, a dynamic structure that evolves until final constriction of the cell. Therefore, molecules able to inhibit its activity will eventually disrupt bacterial viability. In this work, we report a new series of small molecules able to replace GTP and to specifically inhibit FtsZ, blocking the bacterial division process. These new synthesized inhibitors interact with the GTP-binding site of FtsZ (K_d = 0.4−0.8 μM), display antibacterial activity against Gram-positive pathogenic bacteria, and show selectivity against tubulin. Biphenyl derivative **28** stands out as a potent FtsZ inhibitor (K_d = 0.5 μM) with high antibacterial activity [MIC (MRSA) = 7 μM]. In-depth analysis of the mechanism of action of compounds **22**, **28**, **33**, and **36** has revealed that they act as effective inhibitors of correct FtsZ assembly, blocking bacterial division and thus leading to filamentous undivided cells. These findings provide a compelling rationale for the development of compounds targeting the GTP-binding site as antibacterial agents and open the door to antibiotics with novel mechanisms of action.

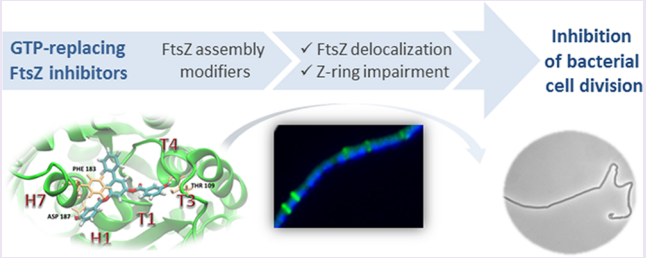

Nosocomial and community-acquired infections associated with antibiotic resistance have become a major public concern at a time when antibacterial drug discovery efforts are declining and the need for effective treatments against new multidrug resistant pathogens continues increasing.[1−4] Methicillin-resistant *Staphylococcus aureus* (MRSA) and glycopeptide resistant enterococci are examples of Gram-positive bacteria that have already shown resistance to the widely prescribed antibiotic vancomycin and other alternatives, such as linezolid and daptomycin.[5,6] The situation is even more concerning for Gram-negative bacteria, where no new drug candidates are currently in advanced clinical development stages.[7] Therefore, we are entering a postantibiotic era with limited treatment options for bacterial infections, highlighting the urgent need for novel-mechanism antimicrobial agents which may help to overcome the antibiotic resistance problem.

In this context, the bacterial cell division protein FtsZ has been proposed as an attractive target for the discovery of new antibacterial agents.[3,8,9] FtsZ is a tubulin-like GTPase highly conserved among bacteria that plays a leading role in the cell division machinery. At the earliest step of cell division, FtsZ undergoes assembly at midcell leading to a dynamic structure known as the Z-ring. Other bacterial division proteins are then recruited to the Z-ring to form the divisome, a complex that finally constricts to generate the two new daughter cells.[10] The functional inhibition of FtsZ by mutations or by cellular protein inhibitors blocks cell division and induces the filamentous phenotype with formation of long undivided bodies instead of the normal bacillar rods.[11] Therefore, small molecules able to inhibit FtsZ activity are expected to block cell division eventually abrogating bacterial viability and hold promise for the development of clinically efficacious antibiotics with an unexplored mode of action.

The structure of FtsZ from diverse bacterial species has been widely studied, showing an N-terminal nucleotide domain and a GTPase activation domain, but with different C-terminal extensions. During FtsZ assembly, the GTPase-activating domain of one subunit contacts the nucleotide site of the subunit below and forms the catalytic pocket, a fact that

Received: July 31, 2014
Accepted: December 8, 2014
Published: December 8, 2014

   dx.doi.org/10.1021/cb500974d | ACS Chem. Biol. 2015, 10, 834−843

underscores the key role of the GTP-binding site in regulating the FtsZ's function. Moreover, the long cleft located between both domains has also been identified as an additional pocket for ligand binding.[12,13]

Over the past decade, several compounds have been shown to inhibit the function of FtsZ by perturbing the protein polymerization and the GTPase activity.[14−17] Some of these molecules have demonstrated antibacterial activity, although their specificity and binding sites have not always been clarified. The reported FtsZ inhibitors include synthetic compounds identified by high-throughput screening or specifically designed, natural products, previously known antibacterial agents and compounds derived from the tubulin field. Regarding synthetic inhibitors, PC190723 is the most studied compound so far.[13,18−20] This difluorobenzamide derivative is an FtsZ polymer-stabilizing agent that exhibits potent antibacterial activity [e.g., MIC (MRSA) = 2.8 μM] and acts as a selective bactericide. Notably, it is the first inhibitor shown to be efficacious in an *in vivo* model of bacterial infection. Later optimization of PC190723 led to drug candidates with superior antibacterial potencies and improved pharmacokinetic profiles.[21,22] The X-ray structure of the complex of PC190723 with *Staphylococcus aureus* FtsZ has allowed the identification of its binding site located between the two domains of FtsZ and suggested that the interaction of the ligand in this cleft modulates the conformational switch that enables the assembly of the protein.[12,13,23,24] Among the natural products, chrysophaentin A[25] and its synthetic hemichrysophaentin analog[26] block the protein assembly in the 10−50 μM range and display broad spectrum antibacterial activity toward Gram-positive bacteria pathogens such as MRSA. On the other hand, C8-substituted GTP analogs inhibit FtsZ polymerization while supporting tubulin assembly, confirming that selective inhibition of the GTP-binding site is possible without unwanted side effects in eukaryotic tubulin.[27] However, these GTP derivatives lack antibacterial activity probably due to poor penetration across the bacterial cell envelope.

As part of an antibiotic discovery program aimed at the identification of new inhibitors of bacterial cell division targeting the GTP-binding site of FtsZ, we identified synthetic compounds UCM05 (**1**) and UCM64 (**2**) by docking our in-house library into the GTP-pocket of *Bacillus subtilis* FtsZ (Bs-FtsZ) and testing the resulting hits in a *mant*-GTP fluorescence anisotropy competitive assay (Supporting Information Table S1). An initial biological evaluation of hit **1** and its analog UCM44 (**3**) showed that they specifically bind to Bs-FtsZ monomers with micromolar affinity (K_d = 2.3 and 0.7 μM, respectively).[28] Molecular dynamics (MD) simulations predicted that one of the phenolic rings of these compounds replaces the interactions made by the GTP phosphates whereas the naphthalene scaffold and the other polyhydroxy phenyl group overlap with the nucleobase. Inhibitors **1** and **3** perturb normal assembly of the protein, impairing the localization of FtsZ into the Z-ring and blocking bacterial cell division [MIC (*B. subtilis*) = 100 and 25 μM, respectively]. These findings prompted us to carry out a deeper exploration around these compounds in order to obtain FtsZ inhibitors with improved antibacterial properties and gain further insight into their mechanism of action on bacterial cells.

Therefore, in this work, we have focused our efforts on the identification of new small molecules that replace the natural regulator GTP and block the bacterial cell division process by specifically inhibiting FtsZ. Starting from inhibitors **1** and **2**, a series of new compounds was synthesized. Their affinity for the GTP-binding site, antibacterial activity against Gram-positive pathogens, and selectivity toward tubulin were assessed. Finally, the bacterial cytological profile of the effective inhibitors was characterized. These compounds inhibit FtsZ assembly and block bacterial cytokinesis, eventually impairing bacterial cell division. The results presented herein provide a promising starting point for the development of new FtsZ GTP-replacing antibacterials that act with a novel mechanism of action.

RESULTS AND DISCUSSION

Essential Chemical Features and Activity-Affinity Correlation of GTP-Replacing FtsZ Inhibitors. In the search of new inhibitors of FtsZ targeting the GTP-binding site, initial hits **1** and **2** were selected as the best candidates in terms of protein affinity and antibacterial activity (Supporting Information Table S1). These compounds share a general structure of two gallate subunits bound to a central core of 1,3-naphthalene or 3,5-biphenyl by ester groups. In order to carry out a structure−activity analysis, the gallate rings and the ester spacers were considered as the two moieties amenable to structural modifications (Figure 1A), since derivatives bearing different

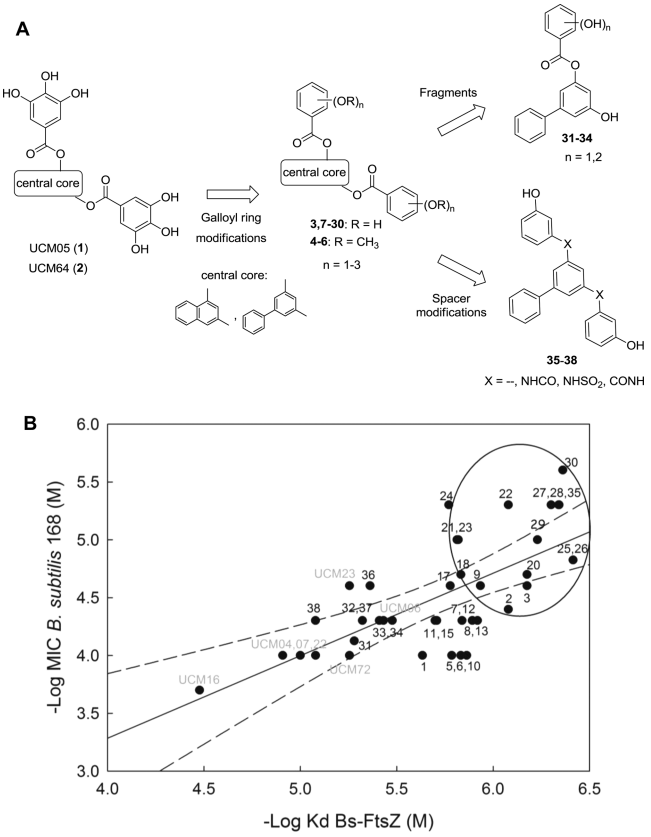

Figure 1. Chemical strategy and activity-affinity analysis for the identification of new FtsZ inhibitors. (A) Chemical structures of compounds **1**−**38**. (B) Correlation between MIC and FtsZ affinity. Other compounds from the in-house library (Supporting Information Table S1) and UCM16 (ref 28) are shown in gray. Correlation coefficient r^2 = 0.50; slope = 0.7 ± 0.1. The solid line is the least-squares linear fit, and dashed lines correspond to 95% confidence intervals.

central cores were already included in our in-house library and displayed less affinity and/or antibacterial activity than the 1,3-naphthalene or 3,5-biphenyl counterparts (Supporting Information Table S1). We first explored the gallate subunits by replacing

dx.doi.org/10.1021/cb500974d | ACS Chem. Biol. 2015, 10, 834−843

Table 1. FtsZ Affinity and Antibacterial Activity of Compounds 1−38

	Compd	R^1	R^2	R^3	R^4	R^5	R^6	K_d[a] FtsZ (μM)	MIC[b] (μM)	
									B. subtilis	MRSA[c]
	1	OH	OH	OH	OH	OH	OH	2.3 ± 0.1[d]	100[d]	60
	3	OH	H	OH	OH	OH	H	0.7 ± 0.2[d]	25[d]	50
	4	OCH_3	OCH_3	OCH_3	OCH_3	OCH_3	OCH_3	> 300	>200	>100
	5	OCH_3	OCH_3	OCH_3	OH	OH	OH	1.5 ± 0.2	100	100
	6	OH	OH	OH	OCH_3	OCH_3	OCH_3	1.6 ± 0.3	100	100
	7	OH	OH	OH	OH	OH	H	1.5 ± 0.1	50	100
	8	OH	OH	OH	OH	H	OH	1.3 ± 0.1	50	100
	9	OH	OH	H	OH	OH	OH	1.2 ± 0.1	25	100
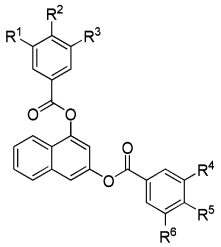	**10**	OH	H	OH	OH	OH	OH	1.4 ± 0.2	100	100
	11	OH	OH	OH	OH	H	H	2.0 ± 0.1	50	100
	12	OH	OH	OH	H	OH	H	1.5 ± 0.1	50	100
	13	OH	H	H	OH	OH	OH	1.3 ± 0.1	50	100
	14	H	OH	H	OH	OH	OH	2.0 ± 0.1	>50	100
	15	OH	OH	H	OH	OH	H	2.0 ± 0.1	50	>100
	16	OH	OH	H	OH	H	OH	0.9 ± 0.1	>50	50
	17	OH	H	OH	OH	H	OH	1.6 ± 0.1	25	10
	18	OH	H	OH	OH	H	H	1.5 ± 0.1	20	10
	19	OH	H	OH	H	OH	H	2.2 ± 0.1	>50	8
	20	OH	H	H	OH	OH	H	0.7 ± 0.2	20	10
	21	OH	H	H	OH	H	H	1.5 ± 0.1	10	10
	22	OH	H	H	H	OH	H	0.8 ± 0.2	5	5
	23	H	OH	H	OH	H	H	1.5 ± 0.1	10	5
	24	H	OH	H	H	OH	H	1.7 ± 0.1	5	5
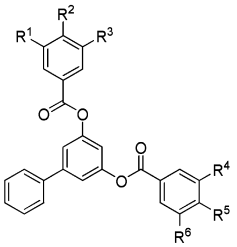	**2**	OH	OH	OH	OH	OH	OH	0.8 ± 0.1	40	50
	25	OH	OH	H	OH	H	OH	0.4 ± 0.1	15	50
	26	OH	OH	H	OH	H	H	0.4 ± 0.1	15	50
	27	OH	H	OH	OH	H	H	0.5 ± 0.1	5	5
	28	OH	H	H	OH	H	H	0.5 ± 0.1	5	7
	29	OH	H	H	H	OH	H	0.6 ± 0.2	10	5
	30	H	OH	H	H	OH	H	0.4 ± 0.1	2.5	5
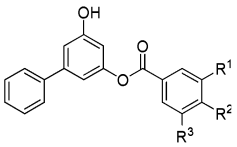	**31**	OH	OH	H	-	-	-	5.3 ± 1.0	75	50
	32	OH	H	OH	-	-	-	5.3 ± 1.0	50	50
	33	OH	H	H	-	-	-	3.8 ± 1.3	50	50
	34	H	OH	H	-	-	-	3.3 ± 0.6	50	50

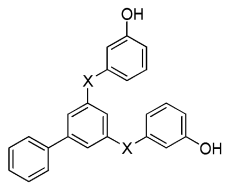	Compd	X	K_d[a] (μM) FtsZ	MIC[b] (μM)	
				B. subtilis	MRSA[c]
	35	-	0.5 ± 0.1	5	3
	36	NHCO	4.3 ± 1.5	25	50
	37	$NHSO_2$	4.8 ± 0.5	50	50
	38	CONH	8.3 ± 1.4	50	50

[a]Values are the mean ± SEM. [b]Minimal concentrations completely inhibiting bacterial growth (MIC). [c]*S. aureus* community acquired methicillin resistant ATCC Nr: BAA-1556 (Institute Pasteur, France) MRSA USA300. [d]Values from ref 28.

hydroxy with methoxy groups (**4**−**6**) or reducing the number of these substituents in compounds **3** and **7**−**30**. Next, elimination of one of the polyhydroxybenzoate systems (monoesters **31**−**34**) and removal or replacement of the ester spacers by other linkers (derivatives **35**−**38**) was considered (Figure 1A, Table 1).

Target compounds **1**−**38** were synthesized by standard synthetic methods (see Supporting Information Figures S1 and S2). Their solubility in aqueous buffer was determined spectrophotometrically following ultracentrifugation,[28] and they were then evaluated using the *mant*-GTP competitive assay[29] to

dx.doi.org/10.1021/cb500974d | *ACS Chem. Biol.* 2015, 10, 834−843

measure their binding affinity for Bs-FtsZ (Table 1). A simple model of inhibitor and *mant*-GTP binding to the same site was applied,[29] from which the best-fitted value of dissociation equilibrium constant, K_d, was determined for each compound (Table 1; see Supporting Information Figure S3 for displacement isotherms). All naphthalene derivatives (**3**−**24**), except the hexamethoxy analog **4**, were able to displace *mant*-GTP, showing better affinity values (K_d = 0.7−2.2 μM) than initial hit **1** (K_d = 2.3 μM). The loss of affinity observed for compound **4** (K_d > 300 μM) is probably due to the absence of free hydroxy groups, since the binding to FtsZ was recovered when one of the original gallate rings was kept (**5** and **6**, K_d = 1.5 and 1.6 μM, respectively). In general, the reduction in the number of hydroxy groups of both phenyl rings improves the binding affinity (**3**, **7**−**24**), and the best K_d values were obtained for those compounds having four or less hydroxyls (**3**, **16**, **20**, and **22**, K_d = 0.7−0.9 μM). Subsequently, only biphenyl analogs bearing one or two hydroxy substituents in each phenyl ring were considered in new derivatives **25**−**30**. In this series, all synthesized compounds displayed submicromolar affinity for the GTP-binding site of FtsZ (K_d = 0.4−0.6 μM), confirming that the scaffold of 3,5-biphenyl is more favorable as a central core than the 3,5-naphthalene system [e.g., K_d (**24**) = 1.7 μM vs K_d (**30**) = 0.4 μM]. Although one or two hydroxy groups seem to be the optimal number of these substituents in each phenyl ring for FtsZ affinity, the position of these substituents did not exert a significant effect. Removal of one of the polyhydroxybenzoate rings in the biphenyl derivatives gave monoesters **31**−**34** that have 10-fold reduced affinity (K_d = 3.3−5.3 μM). Next, derivatives of the high-affinity compound **28** in which the ester bond linkers were replaced by amide, sulfonamide, or retroamide moieties were also studied (**36**−**38**) considering the good results obtained for **28**, which will be discussed in more detail later. The biochemical evaluation of **36**−**38** (Table 1) showed that they maintain affinity for FtsZ (K_d = 4.3−8.3 μM), indicating that the spacers of this new identified chemotype can also be modified. Notably, removal of the linker afforded the high affinity compound **35** (K_d = 0.5 μM) with a carbon−carbon single bond between the central core and the phenol rings.

The antibacterial activity of compounds **1**−**38** was assessed against *B. subtilis* and MRSA USA300 as a representative strain of community acquired resistant Gram-positive bacteria (Table 1). In general, compounds **3**−**30** showed minimal inhibitory concentration (MIC) suppressing growth values in the micromolar range, and the reduction in the number of hydroxy groups was favorable in terms of potency, as previously observed for FtsZ affinity. Thus, **17**−**24** and **27**−**30** are the most potent derivatives [MIC (MRSA) = 5−10 μM]. On the other hand, antibacterial activity of monoacyl fragments **31**−**34** was reduced when compared with their corresponding diesters [e.g., MIC (*B. subtilis*, **28**) = 5 μM vs MIC (*B. subtilis*, **33**) = 50 μM]. Derivatives **36**−**38** also exerted antibacterial activity against both Gram-positive strains [MIC (*B. subtilis*) = 25−50 μM, MIC (MRSA) = 50 μM]. Interestingly, compound **35** displayed high antibacterial activity against MRSA (MIC = 3 μM).

Notably, the logarithmic representation of antibacterial activity in *B. subtilis* (MIC) vs the FtsZ affinity (K_d) values of active compounds within this new series, together with our in-house library hits (Supporting Information Table S1) and naphthyl fragment UCM16 (4-hydroxy-2-naphthyl 3,4,5-trihydroxybenzoate)[28] provided a clear correlation (Figure 1B). This empirical observation supports targeting of FtsZ in the bacterial cells, although it does not prove causality.[3] For instance, similar correlations have been previously employed to predict the tumor cell growth inhibitory potency of epothilones and other microtubule-stabilizing antitumor agents from their affinity for binding to microtubules[30,31] as well as to optimize taxanes.[32]

In summary, the best naphthyl inhibitor combining high affinity and antibacterial activity was compound **22**, whereas in the biphenyl series derivatives **27**−**30** and **35** stand out.

Binding Specificity and FtsZ-Inhibitor Model Complexes. Different experiments were carried out in order to confirm the binding specificity of our compounds. We easily avoided the interference of aggregates formed above inhibitor solubility limits in our competitive binding measurements, which would obstruct the *mant*-GTP fluorescence anisotropy measurements (by scattering highly polarized excitation light) giving artifactually high anisotropy values that grow instead of decreasing with the inhibitor concentration. To further validate specific binding to FtsZ rather than the formation of colloids that nonspecifically bind and inactivate the protein,[15] we subjected solution aliquots of several representative inhibitors to high speed ultracentrifugation (358 000*g*, 20 min at 25 °C) immediately before measuring the inhibition of *mant*-GTP binding by fluorescence anisotropy. Similar results were obtained with the supernatants and noncentrifuged solutions of compounds **22**, **28**, **33**, and **36** (see Supporting Information Figure S4), thus ruling out the formation of large aggregates by these inhibitors that could nonspecifically inhibit nucleotide binding to FtsZ. We note that *mant*-GTP displacement by each inhibitor could be fitted by a competitive binding model and that the data reached full inhibition as allowed by compound solubility (see Supporting Information Figure S3).

The binding of compound **28** to Bs-FtsZ was directly monitored by simultaneously measuring the sedimentation velocity of the protein and the ligand in analytical ultracentrifugation (AUC) experiments (see Supporting Information Figure S5). Compound **28** cosedimented with FtsZ enhancing the formation of protein oligomers; both binding of **28** and FtsZ oligomerization were suppressed by GDP, suggesting that the specific binding of **28** into the nucleotide site induces FtsZ association. Overall, we did not observe any indication of the formation of an FtsZ-nucleotide-inhibitor complex, which suggests mutually exclusive binding. The available results thus support our inhibitors binding into the nucleotide binding pocket of FtsZ, although we could not absolutely rule out the possibility of strong allosteric inhibition with mechanistic studies in the absence of structural information.

To gain structural insight into the potential binding modes of these FtsZ inhibitors, we selected biphenyl **28** as a representative compound to carry out docking studies into the GTP binding site that were further validated by MD simulations. Glide (version 6.3, Schrödinger, LLC, New York, NY, 2014)[33] was used for docking using the extra precision algorithm. The best docking solutions were subjected to MD simulations using Desmond (version 3.8, D. E. Shaw Research, New York, NY, 2014) and the OPLS-2005 force field[34,35] to confirm the ligand stability in the nucleotide binding site (see details in the Supporting Information). In our model, the biphenyl moiety is located in a hydrophobic pocket between helices H5 and H7, whereas one of the hydroxybenzoyl rings interacts with glycine rich loops T1 and T3 and the other is sandwiched between H1 and H7 (Figure 2A). These binding regions overlap with the sugar, phosphate, and guanine ring binding locations, respectively, that have been observed in the crystal structure and analyzed in previous simulation studies[28,29] (see also Supporting Information Figure S6).

dx.doi.org/10.1021/cb500974d | *ACS Chem. Biol.* 2015, 10, 834−843

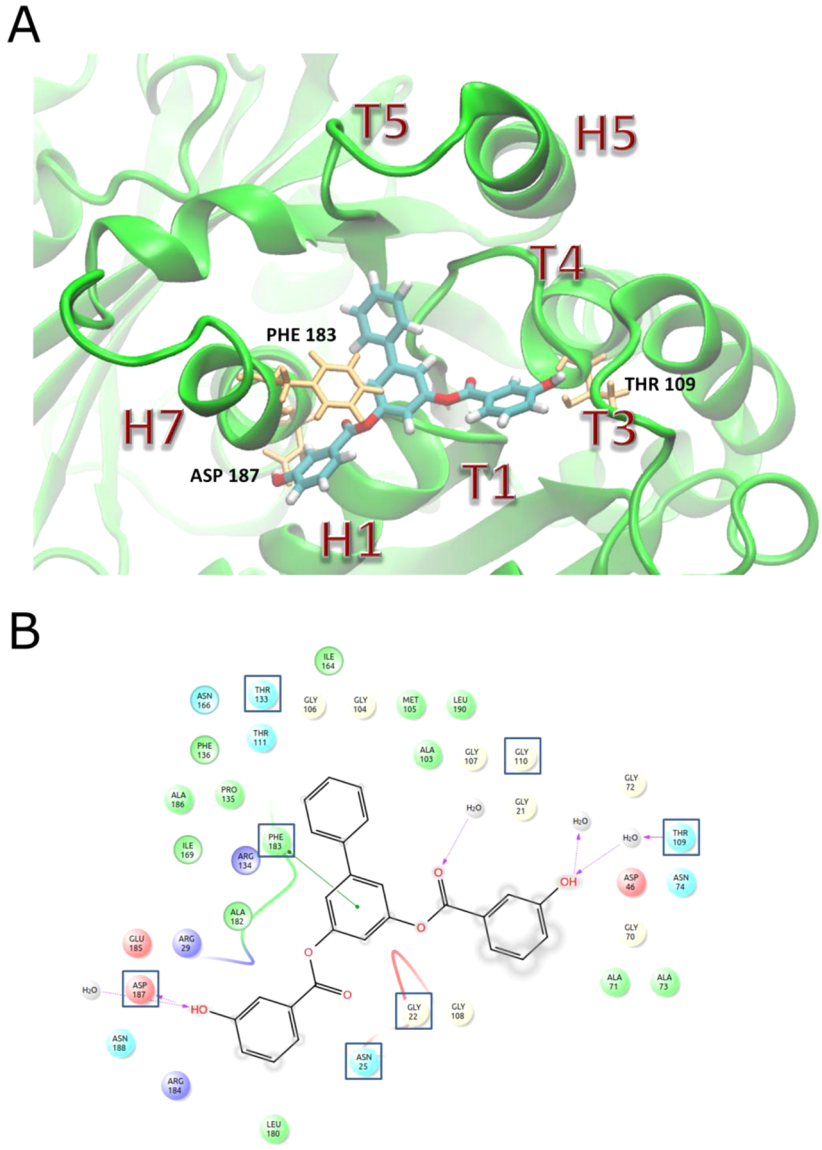

Figure 2. Molecular model of compound **28** recognition by the FtsZ nucleotide binding site. (A) Representative MD snapshot of the binding mode of the simulation of the best docking solution for **28**. (B) Ligand interaction diagram of residues located in the binding site (≤5 Å from the ligand). The amino acid color stands for hydrophobic (green), glycine (gray), polar (light blue), positively charged (magenta), and negatively charged (red). The purple arrows represent H-bonds, and green lines correspond to $\pi-\pi$ interactions. The shadowed atoms indicate solvent exposure, and the shared key residues for GDP binding are marked with squares.

In fact, the most stable contacts observed in **28** shared key binding residues of the natural GDP binder (marked with squares in Figure 2B). Particularly interesting interactions are the ring stack of Phe183 with the biphenyl that mimics guanine stacking and the hydrogen bond of one hydroxy group with Asp187 also observed to be crucial for nucleotide binding. The hydroxybenzoyl moiety located at the phosphate binding region is rather exposed to the solvent, suggesting a weaker interaction with respect to the other hydroxybenzoyl arm. Noticeably, the main interaction partner of this arm, loop T3, is highly flexible as it has been observed in previous simulations with monomeric apo and GDP FtsZ structures.[28] The binding mode obtained for biphenyl **28** is in agreement with those reported for naphthyl derivatives **1** and **3**,[28] although the larger steric volume of **28** results in higher exposure to the solvent. Despite this difference, biphenyl and naphthyl inhibitors share the same interaction mechanism from the modeling point of view. Therefore, these ligand binding model complexes outline a potential inhibition mechanism as they can impair the FtsZ filament dynamics by replacing the common interactions made by GTP and thus inhibit bacterial division.

Microbiological Profile of Selected Inhibitors. Taking together the results obtained with compounds **1**−**38**, we selected for further studies the newly identified high-affinity inhibitors **18**, **20**−**23**, **25**-**30**, and **35** ($K_d \leq 1.5$ μM) endowed with good antibacterial activity (MIC in *B. subtilis* and MRSA ≤ 50 μM). These compounds are encircled at the top right side of the correlation plot between MIC and FtsZ affinity—excluding compound **9** with MIC (MRSA) = 100 μM—(Figure 1B). Fragments **32** and **33** and nonester analogs **36**−**38** were also included together with initial hits **1**−**3**. Their microbiological profile on a panel of antibiotic-resistant pathogenic bacteria was determined (Table 2). In general, all compounds inhibited the growth of Gram-positive resistant pathogenic bacteria such as

dx.doi.org/10.1021/cb500974d | *ACS Chem. Biol.* 2015, 10, 834−843

Table 2. Antibacterial Profile, FtsZ and Tubulin Assembly Inhibition, Bacterial Cell Division Inhibition, and Z-ring Impairment by Selected FtsZ Inhibitors

	MIC (μM)						
compd	MRSA Mu50[a]	*E. faecalis*[b]	*L. monoc.*[c]	FtsZ inhibition at 25 μM[d] (%)	tubulin inhibition at 100 μM[d] (%)	cell division inhibition *B. subtilis* 168 (μM compd.)[e]	Z-ring impairment *B. subtilis* SU570 (μM compd.)[f]
1	80	>100	50	1	98	50[g]	40[g]
2	50	>100	50	16	1	20	20
3	50	100	50	23	19	12[g]	12[g]
18	10	50	10	46	0	no	5
20	10	50	10	34	94	no	nd
21	10	50	50	46	1	no	2
22	5	50	5	21	24	5	5
23	5	50	5	26	0	no	5
25	50	50	50	33	1	8	8
26	50	50	>100	21	5	8	8
27	5	50	7	48	35	3	2
28	7	50	7	36	0	4	3
29	5	50	5	25	0	5	2
30	5	50	5	12	0	3	2
32	50	100	50	26	1	25	12
33	50	50	50	65	48	25	25
35	3	>100	5	55	8	3	no
36	50	>100	50	56	13	12	12
37	50	>100	50	70	78	12	12
38	50	10	50	75	0	12	12

[a]Methicillin, ampicillin, and kanamycin resistant Mu50/ATCC 700699. [b]*Enterococcus faecalis,* gentamicin, and vancomycin resistant V583 ATCC700802 (sequenced strain). [c]*Listeria monocytogenes,* EGDe (sequenced strain). [d]Inhibition of the assembly of purified FtsZ (standard error ±8%) or tubulin (standard error ±9%) employing sedimentation assays (see Figure 2 and Methods). [e]Concentration of compound that produced undivided cells after 2−3 h of incubation. [f]Concentration of compound that produced a significant Z-ring impairment after 1 h of incubation determined by microscopy of live *B. subtilis* SU570 cells expressing FtsZ-GFP as the only FtsZ protein. [g]Values from ref 28. No, negative; nd, not determined.

MRSA (MIC = 3−50 μM) and *Listeria monocytogenes* (MIC = 5−50 μM), while derivatives **18**, **20**−**23**, **25**−**30**, **33**, and **38** were also able to inhibit *Enterococcus faecalis* growth. It is noteworthy to point out **38** as the best inhibitor toward the latter strain (MIC = 10 μM), which is resistant to gentamicin and vancomycin antibiotics. In addition, the best naphthyl and biphenyl compounds **22** and **28** also showed bactericidal activity in MRSA, both with a 10 μM minimal bactericide concentration. Regarding Gram-negative bacteria, although initial biphenyl hit **2** showed moderate activity in resistant *Pseudomonas aeruginosa* and *Escherichia coli* (MIC = 50 μM), none of its derivatives seemed to affect Gram-negative pathogens at the assayed concentration range (MIC > 100 μM), which indicates that removal of hydroxy groups is detrimental for the antibacterial activity against these strains. However, given the high degree of conservation of the nucleotide binding site among FtsZ from different species,[36] development of GTP-replacing FtsZ inhibitors active on Gram-negative bacteria should in theory be possible.[26]

In order to determine whether new identified inhibitors were stable in the whole bacteria assay, the stability of representative compounds **28**, **35**, and **36** in a bacterial culture of *B. subtilis* was assessed, and the 90% remaining compound was quantified by liquid chromatography coupled to mass spectrometry (LC-MS) after 18 h in all cases.

Selective Inhibitors of FtsZ vs Tubulin Assembly. Considering that effective antibacterial compounds targeting FtsZ should avoid unwanted interactions with its eukaryotic homologue tubulin, we screened the ligands for their effects on FtsZ polymerization and tubulin assembly near the maximal concentrations permitted by the least soluble compounds in the presence of each protein (25 and 100 μM compound, respectively; Table 2). All tested derivatives were found to inhibit the GTP-induced polymerization of FtsZ more effectively than their parental compounds **1** and **2** in this *in vitro* assay, **33** and **35**−**38** being the most potent inhibitors, with inhibition percentages higher than 50% at 25 μM. The extent of FtsZ inhibition was apparently uncorrelated with binding affinity or with MIC values. Notwithstanding the higher sensitivity of the tubulin inhibition test, compounds **2**, **18**, **21**, **23**, **25**, **28**−**30**, **32**, and **38** do not inhibit tubulin assembly at 100 μM, whereas **3**, **22**, **26**, **35**, and **36** were considered weak tubulin inhibitors (<25%). Only parent compound **1** and derivatives **20**, **27**, **33**, and **37** cross-inhibit tubulin polymerization (>25%; Table 2). These results constitute a proof of principle that it is possible to selectively inhibit FtsZ with synthetic GTP-replacing compounds that are inactive on tubulin assembly. The inhibition of FtsZ vs tubulin assembly with varying concentrations of structurally representative inhibitors **22**, **28**, **33**, and **36** was also assessed (Supporting Information Figure S7). It can be observed that these compounds inhibit FtsZ polymerization to different extents in a concentration dependent manner when compared with controls, in the presence of a GTP regeneration system. Regarding tubulin inhibition, compound **28** was confirmed to be completely inactive against tubulin up to 100 μM, whereas **22** and **36** are weak tubulin inhibitors and **33** exemplifies stronger inhibition.

In view of the partial inhibition observed in the FtsZ polymer pelleting assay (which measures formation of large protein aggregates irrespective of their structure), we tested the capacity of the compounds themselves to induce the formation of large FtsZ polymers in the absence of GTP (Supporting Information Figure S7).

dx.doi.org/10.1021/cb500974d | *ACS Chem. Biol.* 2015, 10, 834−843

Of note, these inhibitors of the GTP-promoted assembly are able to induce FtsZ aggregation in the absence of GTP, which would justify the typically low percentages observed in the inhibition of FtsZ pelleting. Actually, a lack of ordered FtsZ polymers in these samples was observed by electron microscopy. These observations support our previous proposal from a detailed analysis of the effects of compounds **1** and **3** on FtsZ polymerization.[28] Thus, these inhibitors distort the contacts between FtsZ subunits by binding to the interfacial GTP site, inducing FtsZ aggregates and impairing normal assembly, rather than completely suppressing FtsZ self-association. These *in vitro* results are in line with the observed effects on the cellular localization of FtsZ-GFP described later.

Cytological Profile of Effective FtsZ Inhibitors. In order to identify the most effective bacterial division blockers among our selected FtsZ inhibitors, we examined their effects on the cell division of wild type *B. subtilis* 168 and on FtsZ subcellular localization in *B. subtilis* SU570,[37] a strain that has FtsZ fused to a green fluorescent protein (FtsZ-GFP) as the only FtsZ protein (Table 2). Most of the assayed compounds impaired the position or morphology of the Z-rings. However, **18**, **20**, **21**, and **23** did not block cell division and were not further characterized. Interestingly, compound **35** inhibited bacterial division without showing any effect on the Z-ring, which could suggest an alternative mechanism of action. Excluding these compounds, the minimal compound concentrations that inhibit cell division or impair the Z-ring (Table 2) correlate with the K_d values of binding to FtsZ (Table 1; correlation coefficient r^2 values 0.49 and 0.29, respectively). These cytological observations appear in practice more useful for analyzing inhibitor on-target action than the uncorrelated values of FtsZ *in vitro* polymerization. Representative examples of the most effective Z-ring and bacterial cell division inhibitors that had been shown not to strongly crossreact with tubulin (Table 2) were chosen for further cytological studies (Table 3).

Table 3. Bacterial Phenotype and Cytotoxicity of Effective FtsZ Inhibitors and Analogs

compd	cell division phenotype *B. subtilis* 168	FtsZ-GFP phenotype *B. subtilis* SU570	GI50 IMRO90[e] (μM compd.)	GI50 A549[f] (μM compd.)
1	filamenting[a,b] (50[c])	foci[b,d]	50 ± 10[b]	13 ± 3[b]
2	filamenting[a] (20[c])	foci[d]	60 ± 6	18 ± 3
22	filamenting[a] (5[c])	foci, aberrant rings	34 ± 6	29 ± 5
25	filamenting (8[c])	foci[d]	60 ± 4	47 ± 1
26	filamenting[a] (8[c])	foci[d]	14 ± 3	15 ± 2
28	filamenting[a] (4[c])	few foci, aberrant rings	11 ± 1	13 ± 2
29	filamenting, membrane lysis (5[c])	few foci, aberrant rings	44 ± 6	30 ± 1
30	filamenting, membrane lysis (3[c])	few foci, aberrant rings	50 ± 1	23 ± 1
33	short filaments[a] (25[c])	few foci, few rings	66 ± 3	53 ± 7
36	filamenting[a] (12[c])	few foci, aberrant rings	50 ± 2	36 ± 1

[a]Formation of long undivided cell filaments with intact cell membranes excluding propidiun iodide. [b]Data from ref 28. [c]Concentration of compound (μM) that inhibits cell division; data from Table 2, shown only for comparison. [d]FtsZ forming punctuate foci along cells, with some remaining rings. [e]IMRO90 are lung fibroblast cells. [f]A549 are human lung carcinoma cells.

Cytological profiling of the cell membrane morphology, membrane permeability, and the nucleoid using fluorescence microscopy has recently been shown to distinguish the mode of action of antibiotics targeting the major types of bacterial biosynthetic pathways (DNA, RNA, protein, peptidoglycan and lipid, and subclasses among them), which permits the identification of the mechanism of action of new antibiotics.[38,39] We have thus characterized the cellular effects of our most effective FtsZ inhibitors. Cells of wild type *B. subtilis* 168 exposed to each of these compounds, at lower concentrations than parent compounds **1** and **2**, were significantly longer than control cells (Figure 3 and Table 3). Among them, derivative **28** exhibited the

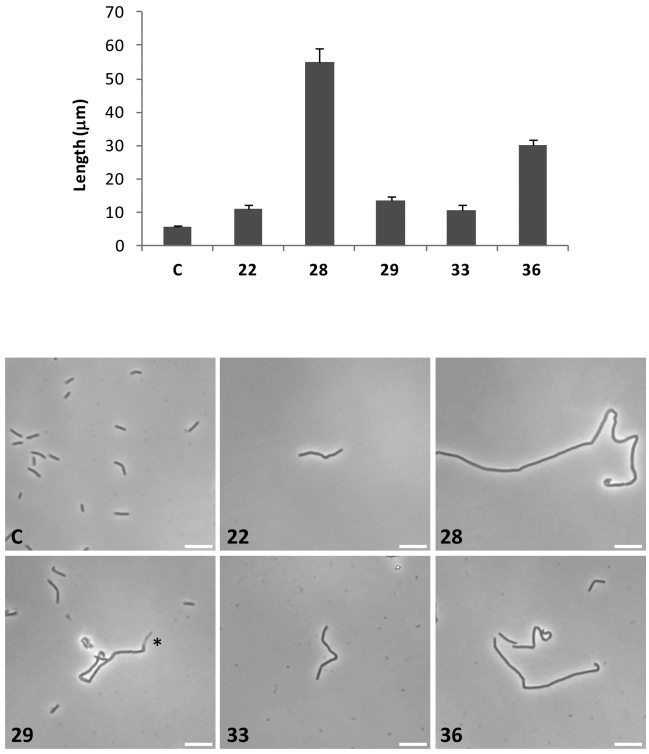

Figure 3. Cell division effect of FtsZ inhibitors. Cells of *B. subtilis* 168 were incubated for 3 h with compounds **22** (5 μM), **28** (4 μM), **29** (5 μM), **33** (25 μM), and **36** (12 μM) and observed by phase-contrast microscopy. Cell length was measured (upper panel), and filamentous undivided cells, significantly longer than in the control ($p < 0.01$), were found with all compounds. A representative example of a filamented cell observed with each compound is shown in the lower panel. Asterisk: region with membrane lysis. Scale bar: 10 μm.

clearest effect on cell division. The phenotype of cells treated with biphenyl **28** (4 μM) consisted of filamentous undivided cells, which had intact membranes excluding propidium iodide. Long filaments were also observed with the amide analog **36** (12 μM), and weaker effects were found with fragment **33** (25 μM) as well as with the naphthyl derivative **22** (5 μM). In addition to filamentation, membrane permeabilization and lysis were observed with compounds **29** and **30** (5 μM and 3 μM, respectively). These results pointed to a second mode of action of these derivatives on bacterial membranes, in addition to targeting FtsZ. While this is an inconvenience for target-based optimization, it might be an advantage for antibacterial effectiveness, since multitargeting may reduce the emergence of resistance mutations in systemic monotherapy. In fact, several antibiotics have a second mode of action,[3] such as the protein synthesis inhibitor aminoglicoside kanamycin, which alters membrane permeability.[38] Moreover, we note that the growth

dx.doi.org/10.1021/cb500974d | ACS Chem. Biol. 2015, 10, 834−843

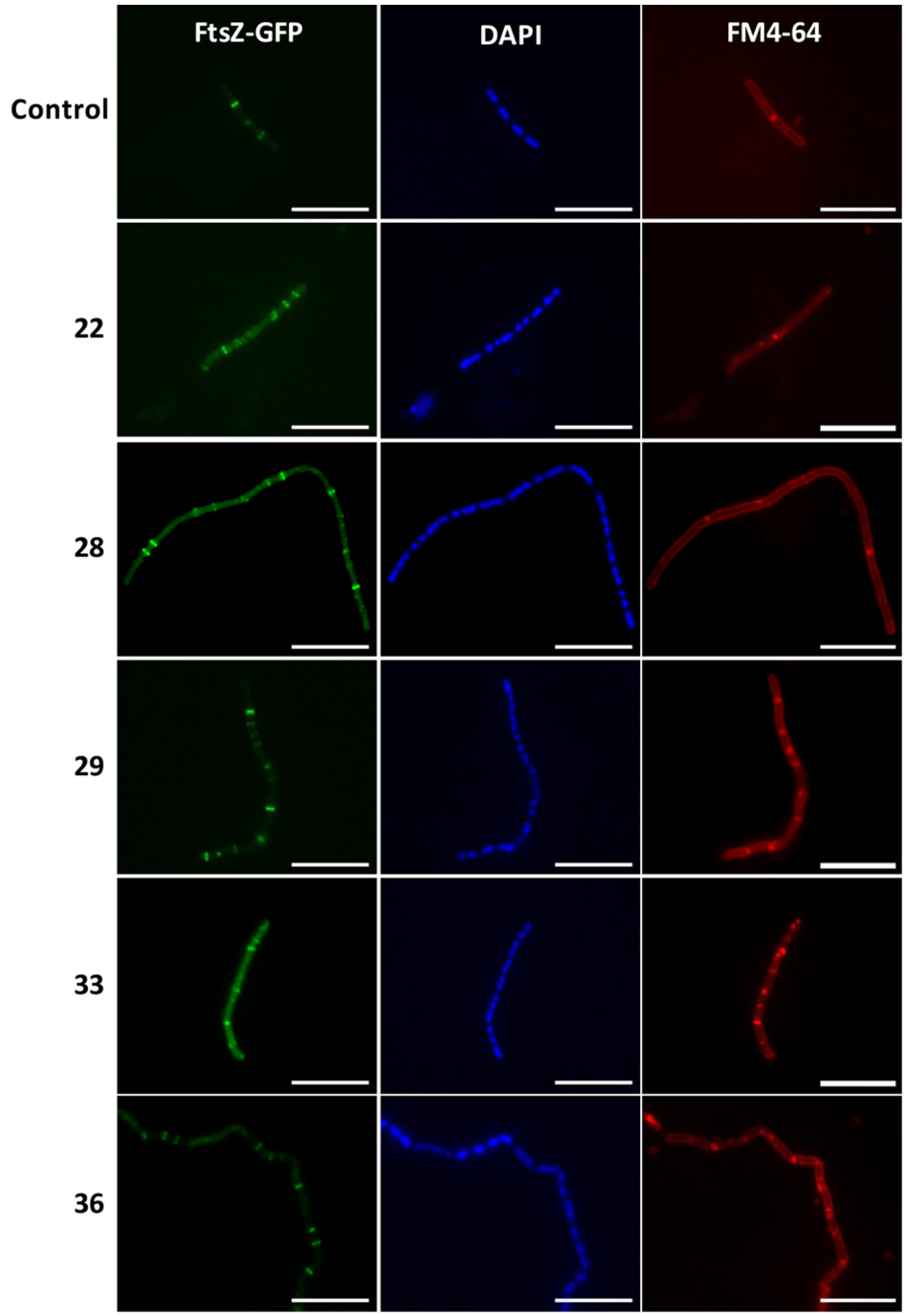

Figure 4. Effect of FtsZ inhibitors on FtsZ subcellular localization. Cells of *B. subtilis* SU570 (FtsZ-GFP) were incubated for 1 h with **22** (5 μM), **28** (3 μM), **29** (2 μM), **33** (25 μM), and **36** (12 μM). FtsZ-GFP, membrane stained with FM4-64 and DNA stained with DAPI were visualized through their corresponding channels with a fluorescence microscope. Scale bar: 10 μm.

inhibitory concentrations of our new FtsZ inhibitors on human lung fibroblasts were typically above the concentrations required for bacterial cell division inhibition (Table 3), supporting potential selectivity against bacterial cells. These compounds were not mitotic inhibitors and their GI50 values on human cells could not be predicted from the observed extents of inhibition of *in vitro* tubulin assembly (Table 2).

Each of these compounds impaired the normal assembly of FtsZ-GFP into the midcell Z-ring prior to division of *B. subtilis* SU570 at concentrations near their MIC values, further supporting FtsZ targeting. The effects observed consisted of a reduction in the proportion of cells with normal Z-rings at division sites with respect to controls and FtsZ delocalization into characteristic punctuate *foci* along the bacterial cells in less than 1 h (Figure 4 and Table 3). Rings along the filamented cells were very frequently observed abnormally close to each other in the presence of compounds **22**, **28**, **29**, and **36**, and FtsZ-GFP *foci* were more abundant in cells treated with compounds **22** and **28**. By contrast, fewer rings and *foci* were observed in cells treated with compound **33**. We independently confirmed the impairment of FtsZ rings and the appearance of *foci* in **28**-treated *B. subtilis* 168 wild type cells by indirect immunofluorescence with polyclonal antibodies against an FtsZ peptide (Supporting Information Figure S8).

dx.doi.org/10.1021/cb500974d | *ACS Chem. Biol.* 2015, 10, 834−843

The impairment of the cell division ring was also reflected in abnormal nucleoid morphology. As opposed to the control cells, nucleoids frequently had a fragmented appearance in cells treated with our FtsZ inhibitors (Figure 4, DAPI column). In many cases, the regions of nucleoid constriction corresponded with Z-rings or FtsZ *foci*, and nucleoid constriction zones where FtsZ-GFP accumulation was not observed could match previous division sites where the Z-ring has already disappeared. Membranes were visualized in the same *B. subtilis* SU570 treated cells with the vital stain FM4-64. In addition to the plasma membrane marking the cell contour and division septa, frequent additional membrane accumulations and patches were observed after treatment with the inhibitors, some of them coinciding with FtsZ *foci* (Figure 4). These observations suggest abortive division sites and plasma membrane lesions. We have compared the effect of **28** with the well studied bacterial cell division inhibitor PC190723,[18−20] which targets another FtsZ binding site.[13] PC190723 (22 μM) also induced the formation of membrane patches that overlap with the characteristic FtsZ *foci* along the undivided cellular filaments (Supporting Information Figure S9). Moreover, we have also observed FM4-64-stained membrane accumulations in *B. subtilis* cells treated with well-known antibacterials such as vancomycin, CCCP, and kanamycin. However, it is important to note that none of these antibacterials led to the observation of long undivided cellular filaments.

In summary, in this work we have identified new small molecules able to specifically inhibit FtsZ with high affinity by replacing the natural regulator GTP. These compounds effectively inhibit protein assembly rather than tubulin polymerization and block bacterial cytokinesis. Furthermore, they display high antibacterial activity against multidrug-resistant Gram-positive pathogenic bacteria. Among them, biphenyl **28** stands out as the most promising FtsZ inhibitor, with good affinity (K_d = 0.5 μM) and antibacterial activity [MIC (MRSA) = 7 μM]. This compound together with **22**, **33**, and **36** acts as an effective FtsZ assembly modifier and leads to filamentous undivided cells, finally disrupting bacterial viability. Overall, these inhibitors contribute to expand the scarce number of GTP mimetics available and provide a compelling rationale for the development of antibacterial agents with novel modes of action.

METHODS

Chemistry. Synthesis and characterization data of final compounds **2**, **4**−**38**, and their corresponding intermediates are fully described in the Supporting Information.

Ligand Competition with *mant*-GTP for Binding to Bs-FtsZ. The fluorescence anisotropy of *mant*-GTP was measured with a Fluoromax-4 (Horiba Jobin Yvon) photon-counting spectrofluorometer, with excitation at 357 nm (5 nm band-pass) and emission at 445 nm (10 nm band-pass) using 2 × 10 mm cells at 25 °C. Ligand competition with *mant*-GTP for binding to FtsZ from *B. subtilis*[28] was performed as described for *Methanococcus jannaschii* FtsZ[29] with modifications. The binding of *mant*-GTP to FtsZ causes a significant increase in its fluorescence that if not taken into account can lead to the calculation of erroneous K_d values when employing anisotropy measurements. To avoid this error, the ratio between the fluorescence intensities of FtsZ-bound and free *mant*-GTP was determined, R = 2.78, and used to correct all anisotropy-based binding calculations. To measure the equilibrium binding constant, *mant*-GTP (200 nM) was titrated with varying concentrations of FtsZ in experimental buffer (50 mM Hepes-KOH, 50 mM KCl, 1 mM EDTA, 10 mM $MgCl_2$, pH 6.8) at 25 °C, which gave a reference binding constant K_b of (9.85 ± 1.05) × 10^5 M^{-1}, an anisotropy value of free *mant*-GTP, r = 0.025 ± 0.005, and the anisotropy of bound *mant*-GTP, r = 0.213 ± 0.002. For the competition measurements, samples (0.5 mL) were prepared by mixing 0.25 mL of *mant*-GTP (1 μM) and binding sites (0.6−1.2 μM) with 0.25 mL buffer without or with competing ligand at varying concentrations, and measurements started 4 min after. The fractional of bound *mant*-GTP and the affinity of the competing ligand were then determined from the fluorescence anisotropy values.[28,29] Controls include samples with GTP, without FtsZ, *mant*-GTP alone, and tested compound alone.

ASSOCIATED CONTENT

Supporting Information

Chemical, computational, and biochemical procedures and biological methods. Table S1 and Figures S1−S9. This material is available free of charge via the Internet at http://pubs.acs.org.

AUTHOR INFORMATION

Corresponding Author

*E-mail mluzlr@quim.ucm.es.

Notes

The authors declare no competing financial interest.

ACKNOWLEDGMENTS

We thank D. Juan for FtsZ purification and Drs. E.J. Harry and M.P. Strauss for the *B. subtilis* strain SU570 and advice. This work was supported by grants from the Spanish Ministerio de Economía y Competitividad (MINECO, SAF2013-48271, SAF2010-22198, BFU2011-23416, BFU2013-44306P and predoctoral fellowships to M.A., L.B.R.-A., A.V., and C.T.) and Comunidad de Madrid (S2010/BMD-2353). E.R.-A. is supported by a predoctoral CSIC-JAE fellowship part-funded by European Social Fund. The authors thank the NMR Core Facilities from Universidad Complutense de Madrid and the computer resources, technical expertise, and assistance provided by the Red Española de Supercomputación.

REFERENCES

(1) Payne, D. J., Gwynn, M. N., Holmes, D. J., and Pompliano, D. L. (2007) Drugs for bad bugs: confronting the challenges of antibacterial discovery. *Nat. Rev. Drug. Discovery 6*, 29−40.

(2) Leclercq, R. (2009) Epidemiological and resistance issues in multidrug-resistant staphylococci and enterococci. *Clin. Microbiol. Infect. 15*, 224−231.

(3) Silver, L. L. (2011) Challenges of antibacterial discovery. *Clin. Microbiol. Rev. 24*, 71−109.

(4) Taiwo, S. S. (2011) Antibiotic-resistant bugs in the 21st century: a public health challenge. *World J. Clin. Infec. Dis. 1*, 11−16.

(5) Gould, I. M., David, M. Z., Esposito, S., Garau, J., Lina, G., Mazzei, T., and Peters, G. (2012) New insights into meticillin-resistant *Staphylococcus aureus* (MRSA) pathogenesis, treatment and resistance. *Int. J. Antimicrob. Agents 39*, 96−104.

(6) Humphries, R. M., Pollett, S., and Sakoulas, G. (2013) A current perspective on daptomycin for the clinical microbiologist. *Clin. Microbiol. Rev. 26*, 759−780.

(7) Butler, M. S., Blaskovich, M. A., and Cooper, M. A. (2013) Antibiotics in the clinical pipeline in 2013. *J. Antibiot. 66*, 571−591.

(8) Lock, R. L., and Harry, E. J. (2008) Cell-division inhibitors: new insights for future antibiotics. *Nat. Rev. Drug Discovery 7*, 324−338.

(9) Vollmer, W. (2006) The prokaryotic cytoskeleton: a putative target for inhibitors and antibiotics? *Appl. Microbiol. Biotechnol. 73*, 37−47.

(10) Adams, D. W., and Errington, J. (2009) Bacterial cell division: assembly, maintenance and disassembly of the Z ring. *Nat. Rev. Microbiol. 7*, 642−653.

(11) Bi, E., and Lutkenhaus, J. (1993) Cell division inhibitors SulA and MinCD prevent formation of the FtsZ ring. *J. Bacteriol. 175*, 1118−1125.

(12) Matsui, T., Yamane, J., Mogi, N., Yamaguchi, H., Takemoto, H., Yao, M., and Tanaka, I. (2012) Structural reorganization of the bacterial

cell-division protein FtsZ from *Staphylococcus aureus*. *Acta Crystallogr. Sect. D: Biol. Crystallogr. 68*, 1175−1188.
(13) Tan, C. M., Therien, A. G., Lu, J., Lee, S. H., Caron, A., Gill, C. J., Lebeau-Jacob, C., Benton-Perdomo, L., Monteiro, J. M., Pereira, P. M., Elsen, N. L., Wu, J., Deschamps, K., Petcu, M., Wong, S., Daigneault, E., Kramer, S., Liang, L., Maxwell, E., Claveau, D., Vaillancourt, J., Skorey, K., Tam, J., Wang, H., Meredith, T. C., Sillaots, S., Wang-Jarantow, L., Ramtohul, Y., Langlois, E., Landry, F., Reid, J. C., Parthasarathy, G., Sharma, S., Baryshnikova, A., Lumb, K. J., Pinho, M. G., Soisson, S. M., and Roemer, T. (2012) Restoring methicillin-resistant *Staphylococcus aureus* susceptibility to beta-lactam antibiotics. *Sci. Transl. Med. 4*, 126ra135.
(14) Kumar, K., Awasthi, D., Berger, W. T., Tonge, P. J., Slayden, R. A., and Ojima, I. (2010) Discovery of anti-TB agents that target the cell-division protein FtsZ. *Future Med. Chem. 2*, 1305−1323.
(15) Anderson, D. E., Kim, M. B., Moore, J. T., O'Brien, T. E., Sorto, N. A., Grove, C. I., Lackner, L. L., Ames, J. B., and Shaw, J. T. (2012) Comparison of small molecule inhibitors of the bacterial cell division protein FtsZ and identification of a reliable cross-species inhibitor. *ACS Chem. Biol. 7*, 1918−1928.
(16) Schaffner-Barbero, C., Martín-Fontecha, M., Chacón, P., and Andreu, J. M. (2012) Targeting the assembly of bacterial cell division protein FtsZ with small molecules. *ACS Chem. Biol. 7*, 269−277.
(17) Foss, M. H., Eun, Y. J., Grove, C. I., Pauw, D. A., Sorto, N. A., Rensvold, J. W., Pagliarini, D. J., Shaw, J. T., and Weibel, D. B. (2013) Inhibitors of bacterial tubulin target bacterial membranes *in vivo*. *Medchemcomm 4*, 112−119.
(18) Haydon, D. J., Stokes, N. R., Ure, R., Galbraith, G., Bennett, J. M., Brown, D. R., Baker, P. J., Barynin, V. V., Rice, D. W., Sedelnikova, S. E., Heal, J. R., Sheridan, J. M., Aiwale, S. T., Chauhan, P. K., Srivastava, A., Taneja, A., Collins, I., Errington, J., and Czaplewski, L. G. (2008) An inhibitor of FtsZ with potent and selective anti-staphylococcal activity. *Science 321*, 1673−1675.
(19) Andreu, J. M., Schaffner-Barbero, C., Huecas, S., Alonso, D., López-Rodríguez, M. L., Ruiz-Avila, L. B., Nunez-Ramirez, R., Llorca, O., and Martin-Galiano, A. J. (2010) The antibacterial cell division inhibitor PC190723 is an FtsZ polymer-stabilizing agent that induces filament assembly and condensation. *J. Biol. Chem. 285*, 14239−14246.
(20) Adams, D. W., Wu, L. J., Czaplewski, L. G., and Errington, J. (2011) Multiple effects of benzamide antibiotics on FtsZ function. *Mol. Microbiol. 80*, 68−84.
(21) Stokes, N. R., Baker, N., Bennett, J. M., Berry, J., Collins, I., Czaplewski, L. G., Logan, A., Macdonald, R., Macleod, L., Peasley, H., Mitchell, J. P., Nayal, N., Yadav, A., Srivastava, A., and Haydon, D. J. (2013) An improved small-molecule inhibitor of FtsZ with superior *in vitro* potency, drug-like properties, and *in vivo* efficacy. *Antimicrob. Agents Chemother. 57*, 317−325.
(22) Kaul, M., Zhang, Y., Parhi, A. K., Lavoie, E. J., and Pilch, D. S. (2014) Inhibition of RND-type efflux pumps confers the FtsZ-directed prodrug TXY436 with activity against Gram-negative bacteria. *Biochem. Pharmacol. 89*, 321−328.
(23) Elsen, N. L., Lu, J., Parthasarathy, G., Reid, J. C., Sharma, S., Soisson, S. M., and Lumb, K. J. (2012) Mechanism of action of the cell-division inhibitor PC190723: modulation of FtsZ assembly cooperativity. *J. Am. Chem. Soc. 134*, 12342−12345.
(24) Ramirez-Aportela, E., Lopez-Blanco, J. R., Andreu, J. M., and Chacon, P. (2014) Understanding nucleotide-regulated FtsZ filament dynamics and the monomer assembly switch with large-scale atomistic simulations. *Biophys. J. 107*, 2164−2176.
(25) Plaza, A., Keffer, J. L., Bifulco, G., Lloyd, J. R., and Bewley, C. A. (2010) Chrysophaentins A-H, antibacterial bisdiarylbutene macrocycles that inhibit the bacterial cell division protein FtsZ. *J. Am. Chem. Soc. 132*, 9069−9077.
(26) Keffer, J. L., Huecas, S., Hammill, J. T., Wipf, P., Andreu, J. M., and Bewley, C. A. (2013) Chrysophaentins are competitive inhibitors of FtsZ and inhibit Z-ring formation in live bacteria. *Bioorg. Med. Chem. 21*, 5673−5678.
(27) Lappchen, T., Pinas, V. A., Hartog, A. F., Koomen, G. J., Schaffner-Barbero, C., Andreu, J. M., Trambaiolo, D., Lowe, J., Juhem, A., Popov, A. V., and den Blaauwen, T. (2008) Probing FtsZ and tubulin with C8-substituted GTP analogs reveals differences in their nucleotide binding sites. *Chem. Biol. 15*, 189−199.
(28) Ruiz-Avila, L. B., Huecas, S., Artola, M., Vergoñós, A., Ramírez-Aportela, E., Cercenado, E., Barasoain, I., Vázquez-Villa, H., Martín-Fontecha, M., Chacón, P., López-Rodríguez, M. L., and Andreu, J. M. (2013) Synthetic inhibitors of bacterial cell division targeting the GTP-binding site of FtsZ. *ACS Chem. Biol. 8*, 2072−2083.
(29) Schaffner-Barbero, C., Gil-Redondo, R., Ruiz-Avila, L. B., Huecas, S., Lappchen, T., den Blaauwen, T., Diaz, J. F., Morreale, A., and Andreu, J. M. (2010) Insights into nucleotide recognition by cell division protein FtsZ from a *mant*-GTP competition assay and molecular dynamics. *Biochemistry 49*, 10458−10472.
(30) Buey, R. M., Diaz, J. F., Andreu, J. M., O'Brate, A., Giannakakou, P., Nicolaou, K. C., Sasmal, P. K., Ritzen, A., and Namoto, K. (2004) Interaction of epothilone analogs with the paclitaxel binding site: Relationship between binding affinity, microtubule stabilization, and cytotoxicity. *Chem. Biol. 11*, 225−236.
(31) Buey, R. M., Barasoain, I., Jackson, E., Meyer, A., Giannakakou, P., Paterson, I., Mooberry, S., Andreu, J. M., and Diaz, J. F. (2005) Microtubule interactions with chemically diverse stabilizing agents: Thermodynamics of binding to the paclitaxel site predicts cytotoxicity. *Chem. Biol. 12*, 1269−1279.
(32) Matesanz, R., Barasoain, I., Yang, C. G., Wang, L., Li, X., De Ines, C., Coderch, C., Gago, F., Barbero, J. J., Andreu, J. M., Fang, W. S., and Diaz, J. F. (2008) Optimization of taxane binding to microtubules: Binding affinity dissection and incremental construction of a high-affinity analog of paclitaxel. *Chem. Biol. 15*, 573−585.
(33) Friesner, R. A., Murphy, R. B., Repasky, M. P., Frye, L. L., Greenwood, J. R., Halgren, T. A., Sanschagrin, P. C., and Mainz, D. T. (2006) Extra precision Glide: Docking and scoring incorporating a model of hydrophobic enclosure for protein-ligand complexes. *J. Med. Chem. 49*, 6177−6196.
(34) Jorgensen, J. H., Swenson, J. M., Tenover, F. C., Barry, A., Ferraro, M. J., Murray, P. R., and Reller, L. B. (1996) Development of interpretive criteria and quality control limits for macrolide and clindamycin susceptibility testing of *Streptococcus pneumoniae*. *J. Clin. Microbiol. 34*, 2679−2684.
(35) Kaminski, G. A., Friesner, R. A., Tirado-Rives, J., and Jorgensen, W. L. (2001) Evaluation and reparametrization of the OPLS-AA force field for proteins via comparison with accurate quantum chemical calculations on peptides. *J. Phys. Chem. B 105*, 6474−6487.
(36) Oliva, M. A., Trambaiolo, D., and Lowe, J. (2007) Structural insights into the conformational variability of FtsZ. *J. Mol. Biol. 373*, 1229−1242.
(37) Strauss, M. P., Liew, A. T. F., Turnbull, L., Whitchurch, C. B., Monahan, L. G., and Harry, E. J. (2012) 3D-SIM super resolution microscopy reveals a bead-like arrangement for FtsZ and the division machinery: implications for triggering cytokinesis. *Plos Biol. 10*, e1001389.
(38) Nonejuie, P., Burkart, M., Pogliano, K., and Pogliano, J. (2013) Bacterial cytological profiling rapidly identifies the cellular pathways targeted by antibacterial molecules. *Proc. Natl. Acad. Sci. U.S.A. 110*, 16169−16174.
(39) Lamsa, A., Liu, W. T., Dorrestein, P. C., and Pogliano, K. (2012) The *Bacillus subtilis* cannibalism toxin SDP collapses the proton motive force and induces autolysis. *Mol. Microbiol. 84*, 486−500.